Impact of the Digital Filter as a Weak Constraint in the Preoperational 4DVAR Assimilation System of Météo-France

PIERRE GAUTHIER* AND JEAN-NOËL THÉPAUT

GMAP–CNRM, Météo-France, Toulouse, France

(Manuscript received 30 June 2000, in final form 1 December 2000)

ABSTRACT

In this paper, a weak constraint formulation of the digital filter based on the Dolph–Chebyshev window is introduced in a preoperational version of the 4DVAR analysis of Météo-France. The constraint is imposed only on the analysis increments to damp spurious fast oscillations associated with gravity–inertia waves. In the incremental formulation of 4DVAR, the analysis increments are obtained from a global model at a uniform low resolution with a simplified set of physical parameterizations, while the high-resolution forecast is obtained with a model that uses a variable-resolution grid having a higher resolution over France and the complete set of physical parameterizations. Both models have the same vertical resolution. In a set of preliminary experiments using the same background field and the same set of observations, it is shown that the weak constraint imposed only on the low-resolution increments manages to control efficiently the emergence of fast oscillations in the resulting high-resolution forecast while maintaining a closer fit to the observations than is possible if the digital filter initialization is applied externally on the final analysis increments. It is also shown that this weak constraint does not add any significant computer cost to the 4DVAR analysis. Finally, 4DVAR has been cycled over a period of 2 weeks and the results show that, compared to 3DVAR, the initial dynamical imbalances are significantly less in 4DVAR even if no constraint is imposed at all. However, it has been noted that the innovation statistics show a positive impact when a constraint is applied.

1. Introduction

The purpose of data assimilation is to blend information contained in observations originating from different sources with information contained in a prior estimate of the state of the atmosphere referred to as the background state. The analysis increments are built by the assimilation and added to the background state to provide new initial conditions out of which the forecast is made. This process however upsets the internal dynamical balance of the model and leads to spurious fast oscillations associated with gravity–inertia waves. To filter out these oscillations, Lynch and Huang (1992) have proposed a simple method based on digital filtering that can filter out fast oscillations as efficiently as nonlinear normal mode initialization. It has the advantage of being easier to implement for limited area models or, as is the case here, a variable resolution global model. There are two problems that arise when using the digital filter. It requires a model integration over a certain period of time, typically 6 h, and a filtered state is only defined at half time. This makes it difficult to assess the impact of the initialization on the analysis. To obtain a filtered state at the analysis time requires some approximations that introduce artificial features into the analysis.

Early on it has been realized by Gustafsson (1992) that in the context of 4DVAR, it would be possible to introduce a weak constraint formulation of the digital filter and to embed it within the 4DVAR cost function so that the constraint is imposed while fitting the observations. Recently, Polavarapu et al. (2000) have pursued this idea both in the context of a weak and a strong constraint approach. Many studies based on the use of the digital filter have applied it directly on the full model state. However, in the context of linear normal mode initialization, Puri et al. (1982) have already shown that this significantly upsets the internal dynamical balance of a model particularly when gravity waves are forced through convection or solar heating. Ballish et al. (1992) have shown that this remains true for nonlinear normal mode initialization and that it is by far preferable to only apply normal mode initialization on the analysis increments in order not to alter the semidiurnal cycle for instance. In the context of operational 3DVAR assimilation systems, this has been shown to lead to better balanced fields (Courtier et al. 1998; Gauthier et al. 1999).

* Permanent affiliation: Data Assimilation and Satellite Meteorology Division, Meteorological Service of Canada, Dorval, Quebec, Canada.

Corresponding author address: Dr. Pierre Gauthier, Data Assimilation and Satellite Meteorology Division, Meteorological Service of Canada, 2121 Trans-Canada Highway, Dorval, PQ H9P 1J3, Canada.
E-mail: pierre.gauthier@ec.gc.ca

In the incremental 4DVAR (Courtier et al. 1994), the cost function is expressed in terms of the analysis increments, the evolution of which is described at a lower resolution with a simplified model. It is then possible to introduce the digital filter initialization as a weak constraint (J_c-DFI) on the low-resolution analysis increments. This paper investigates if this is sufficient to control the emergence of fast oscillations in the subsequent high-resolution forecast. Two different formulations of the weak constraint will be compared: one based on the normal mode formulation and the other on the digital filter. These results are compared with those from an experiment where the digital filter is applied externally on the final analysis increments. After briefly introducing the formulation of a low-pass digital filter in section 2, the incremental form of the weak constraint is introduced in section 3 where it is shown that it can be naturally combined to the computation of the observation component of the cost function. This implies that this constraint is not adding any significant cost to 4DVAR. The experiments presented here were all based on a preoperational version of the 4DVAR assimilation system of Météo-France, which is described in section 4. The first set of experiments used the same background field and the same observations and it was possible to compare different ways of constraining or filtering fast oscillations: these are presented in section 5. Finally, in section 6, 4DVAR was cycled over a period of 2 weeks and those results are compared for four experiments. Particular attention has been paid to the dynamical imbalances of the different analyses.

2. Formulation of a low-pass digital filter

Referring to Lynch and Huang (1992, LH92 hereafter), Hamming (1989), and Lynch (1997), time oscillations exceeding a *cutoff frequency* of $\omega_c = 2\pi/T_c$ can be filtered by applying a digital filter to a time series $f_k \equiv f(t_k)$ for $t_k = k\Delta t$, Δt being the time step. This proceeds by doing a discrete convolution of f_k with a function h_k so that

$$(f^*h)(t_N) = \sum_{k=-\infty}^{k=+\infty} h_k f_{N-k}. \tag{2.1}$$

The *weighting* function h_k is found to be

$$h_k = \frac{\sin\omega_c k\Delta t}{k\pi}.$$

This is referred to as the *idealized low-pass filter*. In NWP, this can be used to obtain initial conditions at $t = t_N = N\Delta t$ leading to a forecast devoid of fast oscillations. As shown in LH92, the digital filter initialization (DFI) is very similar to nonlinear normal mode initialization (NNMI) provided there is a clear separation of frequency between gravity and Rossby modes.

In practice, the convolution (2.1) is restricted to a finite time interval, the time span T_S. In terms of the chosen time step, $T_S = 2M\Delta t$ and (2.1) is approximated by

$$(f^*h)(t_0) = \sum_{k=-M}^{k=+M} h_k f_{-k} \equiv \sum_{k=-M}^{k=+M} \alpha_k f_k, \tag{2.2}$$

with $\alpha_k = h_{-k}$. This truncation introduces Gibbs oscillations that can be attenuated by introducing a *Lanczos window*, which means that the *weights* α_k of the filter are defined as

$$\alpha_k = h_{-k}W_k,$$

with $W_k = [\sin k\pi/(M+1)]/[k\pi/(M+1)]$. An alternative has been proposed by Lynch (1997) to use instead a Dolph–Chebyshev window (or *Dolph* window) in which case

$$W_k = \frac{1}{2M+1}\left[1 + 2r\sum_{m=0}^{M} T_{2M}(x_0\cos\theta_m/2)\cos m\theta_k\right], \tag{2.3}$$

where $1/x_0 = \cos\pi\Delta t/\tau_S$, $1/r = \cosh(2M\cosh^{-1}x_0)$, $\theta_k = k(2\pi/M)$, and T_{2M} is the Chebyshev polynomial of degree $2M$. When used as a window, as proposed and discussed in Lynch (1997), choosing $\tau_S = M\Delta t$ is the most reasonable value in that a larger value does not filter sufficiently the Gibbs oscillations while shorter values have a damping effect on the frequencies in the pass band of the filter. One could also define $\alpha_k = W_k$ as defined by (2.3) by setting $\tau_S = T_c$. This will be referred to as the *Dolph filter*.

The characteristics of the Dolph filter are best understood by looking at the impact the filter has when applied to a single oscillation. The transfer function

$$T(\omega) = \alpha_0 + 2\sum_{k=1}^{M} \alpha_k \cos k\omega\Delta t$$

represents the ratio of the amplitude of the filtered wave to its initial amplitude. The spurious gravity waves that need to be filtered have periods of 6 h or less and the time series needs to be long enough for those to be properly represented. On the other hand, a model must be integrated to generate this time series and one would like to keep this integration as short as possible. When the DFI is applied externally, the objective is then to minimize the time span to reduce the cost while filtering sufficiently the spurious fast oscillations and reducing the dynamical imbalances. As discussed in Lynch et al. (1997), applying the Dolph filter twice is more efficient at reducing fast oscillations than windowed low-pass filters. Figure 1 summarizes the properties of three different configurations of the digital filter by depicting their transfer function. It shows the response for a span of 6 h, a cutoff period of also 6 h for a Dolph window and a stop-band edge $\tau_S = 3$ h for a Dolph filter. It also shows the response of the Dolph filter with a 3.5-h time span and a stop-band edge of 5 h applied twice, which corresponds to the parameters used for the external DFI

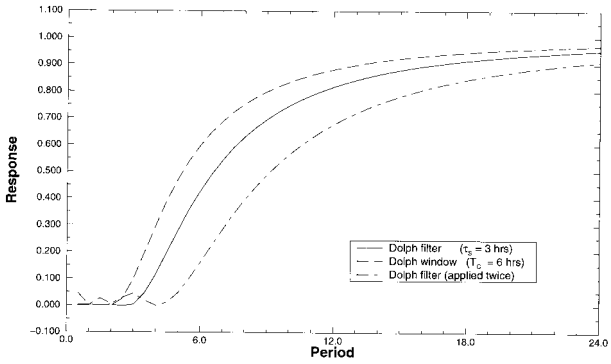

FIG. 1. Transfer function of the digital filter as a function of period. The time step is 900 s, the time span, 6 h: the cutoff period is 6 h for a Dolph window (dashed line) while the pass-band edge is 3 h for the Dolph filter (solid line). The transfer function is also shown for the case where the Dolph filter is applied twice with a pass-band edge of 5 h and a shorter time span of 3.5 h.

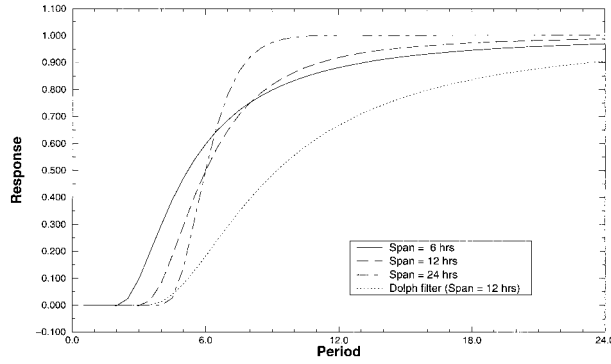

FIG. 2. Transfer functions of the digital filter with a Dolph–Chebyshev window when the time span is 6, 12, and 24 h. The time step is 900 s. The transfer function is also shown for the Dolph filter with a pass-band edge of 3 h and a 12-h time span.

used in our experiments. In all cases, the time step has been set to 900 s, the time step necessary to integrate the model in the experiments to be presented later. The Dolph filter applied twice presents the advantage of filtering more efficiently all waves with periods in between 3 and 6 h. In that respect, it performs better. On the other hand, waves in the pass band are significantly more damped with this filter. However, it must be remembered that the filtering of the waves in the pass band is less damageable when the initialization procedure is applied only to the analysis increment and not to the full analysis (Puri et al. 1982; Ballish et al. 1992; Courtier et al. 1998; Gauthier et al. 1999). This means that if $\mathbf{X}_a$ is the analysis, $\mathbf{X}_b$ the background field, and $\delta\mathbf{X}_a$ the analysis increment, the initialized increment is then defined as

$$\delta_I\mathbf{X} = \mathcal{N}(\mathbf{X}_a) - \mathcal{N}(\mathbf{X}_b),$$

where $\mathcal{N}$ stands for the initialization process. The filtered analysis is then $\mathbf{X}_I = \mathbf{X}_b + \delta_I\mathbf{X}$ so that forced slow waves (like those associated with the semidiurnal cycle and tides) present in the background field are not altered by the initialization. This is what is done in the operational implementation of the DFI at Météo-France.

It is possible to make the digital filter more selective by increasing the span. Figure 2 shows the impact of increasing the time span from 6 to 24 h for the case of the Dolph window with a cutoff period of 6 h. Increasing the time span sharpens considerably the transfer function and brings it closer to the idealized low-pass filter. This figure also shows that the Dolph filter with a pass-band edge of 3 h and a time span of 12 h damps excessively the waves in the pass band. As noted in Lynch (1997), the Dolph filter is not recommended when long time spans are used. In summary, the Dolph window is preferable when long time spans are used while the Dolph filter (applied twice) is more suitable for short time spans.

3. Variational formulation of the digital filter initialization

By reindexing the formulation (2.2) of the digital filter, it can now be rewritten as

$$\overline{\mathbf{X}}(t_{N/2}) = \sum_{k=0}^{N} \alpha_k \mathbf{X}(t_k), \tag{3.1}$$

where $t_0 \le t_{N/2} \le t_N$ and the overbar notation refers to the state being filtered. Following Fillion et al. (1995), the model state is constrained to be filtered at time $t_{N/2}$ and not at the initial time: the filtered trajectory is therefore not defined for $t < t_{N/2}$. For a reference trajectory $\mathbf{X}_R(t)$ considered to be filtered, then $\overline{\mathbf{X}}_R(t_{N/2}) = \mathbf{X}_R(t_{N/2})$ and we are now interested to find a perturbed trajectory $\delta\mathbf{X}(t)$ such that $\mathbf{X}_R(t) + \delta\mathbf{X}(t)$ remains filtered. Under these conditions, it suffices to apply the DFI to $\delta\mathbf{X}(t)$. As discussed in the previous section, even in the context of 3DVAR, it is best to apply the initialization procedure only to the analysis increment and not to the full analysis.

Following Gustafsson (1992) and Polavarapu et al. (2000), the digital filter can be introduced as a weak constraint through a penalty cost function $J_c(\delta\mathbf{X}_0)$ defined as

$$J_c(\delta\mathbf{X}_0) = \frac{1}{2}\langle \delta\mathbf{X}(t_{N/2}) - \delta\overline{\mathbf{X}}(t_{N/2}),\, \delta\mathbf{X}(t_{N/2}) - \delta\overline{\mathbf{X}}(t_{N/2})\rangle, \tag{3.2}$$

where a suitable norm has to be used. The choice of the norm will be discussed later. Working with perturbations allows us to set the problem within the framework of the tangent linear approximation. Here the reference trajectory is considered to be already filtered and the filtered perturbation is then

$$\delta\overline{\mathbf{X}}(t_{N/2}) = \sum_{k=0}^{N} \alpha_k \delta\mathbf{X}(t_k).$$

Moreover, introducing the propagator of the tangent linear model (TLM), $\mathbf{L}(t_0, t_k)$, then

$$\delta\overline{\mathbf{X}}(t_{N/2}) = \sum_{k=0}^{N} \alpha_k \mathbf{L}(t_0, t_k)\delta\mathbf{X}_0,$$

since $\delta\mathbf{X}(t_k) = \mathbf{L}(t_0, t_k)\delta\mathbf{X}_0$. Defining

$$\mathbf{b}_{N/2} = \delta\mathbf{X}(t_{N/2}) - \delta\overline{\mathbf{X}}(t_{N/2}),$$

it follows from (3.2) that

$$\nabla_{\mathbf{x}} J_c(\delta\mathbf{X}_0) = \sum_{k=0}^{N} \gamma_k \mathbf{L}_1^*(t_0, t_k)\mathbf{b}_{N/2}, \tag{3.3}$$

where

$$\gamma_k = \begin{cases} -\alpha_k & \text{if } k \neq N/2 \\ 1 - \alpha_k & \text{if } k = N/2 \end{cases}$$

and $\mathbf{L}_1^*$ is the adjoint of the propagator derived with respect to the norm defining J_c. The gradient can then be obtained through a single backward integration of the adjoint model.

a. Computation of J_c and J_o

If $\mathbf{H}_k$ stands for the observation operator at time t_k, one can express the misfit to the observations as a cost function

$$J_o(\delta\mathbf{X}_0) = \frac{1}{2}\sum_{k=0}^{N} [\mathbf{H}_k'\mathbf{L}(t_0, t_k)\delta\mathbf{X}_0 - \mathbf{y}_k']^{\mathrm{T}} \times \mathbf{R}^{-1}[\mathbf{H}_k'\mathbf{L}(t_0, t_k)\delta\mathbf{X}_0 - \mathbf{y}_k'] \tag{3.4}$$

in its incremental form (Courtier et al. 1994), with $\mathbf{y}_k' = \mathbf{y}_k - \mathbf{H}_k[\mathbf{X}_R(t_k)]$ being the innovation vector. Its gradient is

$$\nabla_{\mathbf{x}} J_o(\delta\mathbf{X}_0) = \sum_{k=0}^{N} \mathbf{L}^*(t_0, t_k)\mathbf{H}_k'^{\mathrm{T}}\mathbf{R}^{-1}[\mathbf{H}_k'\mathbf{L}(t_0, t_k)\delta\mathbf{X}_0 - \mathbf{y}']. \tag{3.5}$$

The adjoint $\mathbf{L}^*(t_0, t_i)$ is derived with respect to an inner product that may not correspond to the one used to define the J_c-DFI. Let $[\mathbf{f}, \mathbf{g}]$ be that particular inner product such that

$$[\mathbf{L}(t_0, t_k)\ \delta\mathbf{x}_0,\ \delta^*\mathbf{x}_0] = [\delta\mathbf{x}_0,\ \mathbf{L}^*(t_0, t_k)\ \delta^*\mathbf{x}_0].$$

In terms of this inner product, the cost function J_c can be expressed as

$$\begin{aligned} J_c(\delta\mathbf{X}_0) &= \frac{1}{2}\langle \delta\mathbf{X}(t_{N/2}) - \delta\overline{\mathbf{X}}(t_{N/2}),\ \delta\mathbf{X}(t_{N/2}) - \delta\overline{\mathbf{X}}(t_{N/2})\rangle \\ &= \frac{1}{2}[\delta\mathbf{X}(t_{N/2}) - \delta\overline{\mathbf{X}}(t_{N/2}),\ \mathbf{Q}(\delta\mathbf{X}(t_{N/2}) - \delta\overline{\mathbf{X}}(t_{N/2}))], \end{aligned} \tag{3.6}$$

where $\mathbf{Q}$ is a positive definite matrix. Consequently, (3.3) is then

$$\nabla_{\mathbf{x}} J_c(\delta\mathbf{X}_0) = \sum_{k=0}^{N} \mathbf{L}^*(t_0, t_k)[\gamma_k \mathbf{Q}\mathbf{b}_{N/2}]. \tag{3.7}$$

The additive nature of the computation of the gradient makes it possible to compute $\nabla_{\mathbf{x}} J_o + \nabla_{\mathbf{x}} J_c$ at virtually the same computational cost as that of computing $\nabla_{\mathbf{x}} J_o$ alone. The matrix $\mathbf{Q}$ is introduced to reconcile the definitions of the norm used for J_o and J_c so that their two gradients can be combined without loss of generality. The use of a different norm for J_c is required and gives flexibility in the application of the constraint as will be now discussed.

b. Choice of norm for J_c

The penalty cost function has to be related to what is considered necessary to be filtered. If $\mathbf{X} = (\Psi, \chi, T, p_s, q)$ with Ψ, χ, T, q, and p_s being, respectively, the streamfunction, velocity potential, temperature, specific humidity, and surface pressure, the moist energy norm can be expressed as

$$\begin{aligned} \langle \mathbf{X}, \mathbf{X}\rangle_E = &\frac{1}{2}\int_0^{p_s} dp \int_S \nabla\Psi \cdot \nabla\Psi\ dS \\ &+ \frac{1}{2}\int_0^{p_s} dp \int_S \nabla\chi \cdot \nabla\chi\ dS \\ &+ \frac{c_p}{T_r}\int_0^{p_s} dp \int_S T^2\ dS + \frac{R_d T_r}{p_r^2}\int_S p_s^2\ dS \\ &+ \varepsilon\frac{L^2}{c_p T_r}\int_0^{p_s} dp \int_S q^2\ dS, \end{aligned} \tag{3.8}$$

where T_r and p_r are constant reference temperature and pressure; and c_p, L, and R_d are, respectively, the specific heat at constant pressure, the latent heat of condensation per unit mass, and the gas constant of dry air. As discussed in Ehrendorfer et al. (1999), this particular choice of norm has the merit of scaling properly the different contributions. By choosing $\varepsilon = 0$ or 1, moisture can be included or not. When applied directly, the digital filter acts uniformly on all variables and all grid points because each is considered to be an independent time series in its treatment. In a variational context, choosing the energy norm will filter first the most energetic fast oscillations.

Finally, the chosen norm can include the penalty constant λ of the weak constraint formulation that could be made to vary with position and variable. This gives flexibility in the application of the constraint. Theoretically, λ should be representative of the expected degree to which the constraint should be imposed. In the remainder of this paper, however, the penalty coefficient, denoted as λ, will be taken as constant.

c. Preconditioning

A complexity arises from the fact that the minimization will see the combined effects of J_b (the background term), J_o, and J_c-DFI. To improve the conver-

gence of the minimization, it is customary to precondition with respect to the background term. This is done by introducing the control variable $\boldsymbol{\xi} = \mathbf{B}^{-1/2}\mathbf{x}$ with $\mathbf{x} = \mathbf{X} - \mathbf{X}_b$, with $\mathbf{B}$ being the background-error covariance matrix. The complete cost function, including the background term, then takes the form

$$J(\boldsymbol{\xi}) = \frac{1}{2}\boldsymbol{\xi}^{\mathrm{T}}\boldsymbol{\xi} + \frac{1}{2}\sum_{k=0}^{N}[\mathbf{H}_k'\mathbf{L}(t_0, t_k)\mathbf{G}\boldsymbol{\xi} - \mathbf{y}_k']^{\mathrm{T}} \times \mathbf{R}^{-1}[\mathbf{H}_k'\mathbf{L}(t_0, t_k)\mathbf{G}\boldsymbol{\xi} - \mathbf{y}_k'] + \lambda J_c(\boldsymbol{\xi}),$$

where $\delta\mathbf{x}_0 = \mathbf{B}^{1/2}\boldsymbol{\xi} + [\mathbf{X}_b - \mathbf{X}_R(t_0)] \equiv \mathbf{G}\boldsymbol{\xi}$ and λ is the penalty constant. Here, the initial conditions of the reference trajectory $\mathbf{X}_R(t_0)$ may differ from the background state. The gradient as seen by the minimizer is then of the form

$$\nabla_{\boldsymbol{\xi}}J = \boldsymbol{\xi} + (\mathbf{B}^{1/2})^{\mathrm{T}}[\nabla_{\mathbf{x}}J_o(\delta\mathbf{X}_o) + \lambda\nabla_{\mathbf{x}}J_c(\delta\mathbf{X}_o)], \quad 3.9$$

with the Euclidean norm being used in ξ space. This preconditioning has therefore a filtering effect on the gradient of J_o and J_c. The current formulation used for $\mathbf{B}$ corresponds to that described in Derber and Bouttier (1999), which implies that the minimization will adjust first the large-scale components of the increments. Due to this filtering of the gradient by the background error covariances, the spectrum of $\delta\mathbf{X}_0$ should be within a horizontal resolution of T95. However, these low-resolution initial conditions can develop small scales during the integration, which may justify the use of a higher resolution for the incremental model (Laroche and Gauthier 1998). The most important justification for the increased resolution is that it represents better the reference trajectory used to define the tangent linear and adjoint models.

4. Description of the 4DVAR system

a. The model

The experiments described in this paper are based on a preoperational version of the 4DVAR system of Météo-France, which is part of the Integrated Forecasting System/Action de Recherche Petite Echelle Grand Echelle (IFS/ARPEGE) developed jointly by Météo-France and the European Centre for Medium-Range Weather Forecasts (ECMWF). The ARPEGE model of Météo-France is a variable-resolution global spectral model obtained by applying a conformal mapping of the sphere onto itself, the Schmidt transform, that makes it possible to concentrate the resolution over a particular area, here over France (Courtier and Geleyn 1988). With a stretching factor of 3.5, a global resolution at a triangular truncation of T199 yields a resolution of approximately 24 km over France, which becomes gradually coarser. The coarsest resolution is equivalent to T42 (~310 km) at the antipodes. The model has 31 vertical levels using a hybrid vertical coordinate. The notation T199L31C3.5 is used to describe the horizontal and vertical resolution. A detailed description of the model can be found in Courtier et al. (1991) and Geleyn et al. (1994).

In the assimilation system of Météo-France that was operational until June 2000, the analysis was obtained with an incremental 3DVAR (Thépaut et al. 1998) similar to that described in Derber and Bouttier (1999) and Courtier et al. (1998). The analysis increments were computed at a uniform resolution of T127L31C1.0. An assimilation cycle is then capable of running continuously because the coarsest resolution of T42 of the model is nevertheless sufficient to resolve the planetary waves. This is discussed in Courtier and Geleyn (1988) who point out that there is a limit to the decrease in resolution.

b. Configuration of the incremental 4DVAR algorithm

When using the incremental formulation of Courtier et al. (1994), the high-resolution model is run and innovations are computed with respect to the resulting high-resolution trajectory. This process is referred to as an *outer iteration.* A degraded lower-resolution model with simplified physics is then used to perform most of the integrations required by the minimization of the approximate cost function: these are referred to as the *inner iterations.* The resulting low-resolution increment is then used to correct the initial conditions of the high-resolution model, which is integrated once more, and the innovations are recomputed with respect to this updated trajectory. This corresponds to an outer iteration also referred to as an *update.* As shown in Laroche and Gauthier (1998), this incremental approach approximates rather well the full 4DVAR problem provided a sufficient number of outer iterations is made. Rabier et al. (2000) have also employed an incremental approach in the operational implementation of 4DVAR at ECMWF.

The design of the incremental 4DVAR requires one to decide how many outer iterations will be performed and what will be the configuration of the model used for the inner iterations. The level of complexity of the simplified model may change between outer iterations. Experiments were carried out at ECMWF and Météo-France and it was found that good results could be obtained with two outer iterations. At Météo-France, the simplified model is T95L31C1.0 with no physics (except for surface drag and vertical diffusion) in the first set of inner iterations while the simplified physics of Janisková et al. (1999) is activated in the second set. In the nomenclature of Veersé and Thépaut (1998), this is indicated as 50/20 meaning that 50 and 20 iterations are made in the first and second inner loop, respectively.

One outer iteration then involves the following sequence of operations.

1) Integration of the model in its operational configuration (T199L31C3.5) including the complete phys-

ics over the assimilation interval [0, T] to obtain a high-resolution trajectory $\mathbf{X}^{(n)}(t)$ used to compute the innovations $\mathbf{d}^{(n)} = \mathbf{y} - \mathbf{H}\mathbf{X}^{(n)}$ for all observations in the interval.

2) Projection of $\mathbf{X}^{(n)}(0)$ to low resolution to define initial conditions $\mathbf{x}^{(n)}(0) = \Pi_L\mathbf{X}^{(n)}(0)$ to integrate the T95L31C1.0 model with the complete physics: the resulting trajectory $\mathbf{x}^{(n)}(t)$ is used to define the tangent linear model. As pointed out in Rabier et al. (2000), this is preferred to a direct projection $\Pi_L\mathbf{X}^{(n)}(t)$ because of differences in the orography used in the low- and high-resolution models. This is even more justified in the present case because the higher-resolution model has a significantly different geometry than the lower-resolution model.
3) Use the tangent linear model and its adjoint with (or without) the simplified physics to perform the minimization of the incremental cost function:

$$J^{(n)}(\boldsymbol{\xi}) = \frac{1}{2}\boldsymbol{\xi}^{\mathrm{T}}\boldsymbol{\xi} + \frac{1}{2}\sum_{k=0}^{N}[\mathbf{H}_k'\mathbf{L}(t_0, t_k)\mathbf{G}\boldsymbol{\xi} - \mathbf{d}_k^{(n)}]^{\mathrm{T}} \times \mathbf{R}^{-1}[\mathbf{H}_k'\mathbf{L}(t_0, t_k)\mathbf{G}\boldsymbol{\xi} - \mathbf{d}_k^{(n)}] + \lambda J_c(\boldsymbol{\xi}), \quad (4.1)$$

where $\boldsymbol{\xi} = \mathbf{B}^{-1/2}\{\delta\mathbf{x}^{(n)}(0) - [\mathbf{x}_b - \mathbf{x}^{(n)}(0)]\}$ and $\mathbf{d}_k^{(n)} = \mathbf{y}_k - \mathbf{H}[\mathbf{X}^{(n)}(t_k)]$. Here the notation $\mathbf{H}$ is used to emphasize that the observation operator is related to the higher-resolution configuration of the model and therefore differs from that used in the lower-resolution incremental model.

4) Interpolate the resulting low-resolution increment $\delta\mathbf{x}^{(k)}(0)$ to the high-resolution grid to obtain $\Delta\mathbf{X}^{(k)}(0) = \Pi_L^{-1}\delta\mathbf{x}^{(k)}(0)$, with Π_L^{-1} being the generalized inverse of Π_L.
5) Update the trajectory and the innovations by integrating the high-resolution model with the initial conditions $\mathbf{X}^{(k+1)}(0) = \mathbf{X}^{(k)}(0) + \Delta\mathbf{X}^{(k)}(0)$.

The assimilation interval used in our experiment is 6 h so that the analysis valid at 0000 UTC is based on all observations within the interval −0300 UTC to +0300 UTC. The initial time referred to above would then be −0300 UTC in this case. The NNMI imposed as a weak constraint in the inner iterations was not sufficient to control the emergence of spurious gravity waves introduced by the significantly different configuration of the inner and outer models. Therefore, in the last outer iteration, it was found necessary to apply an external digital filter initialization on the analysis increments at the initial time as described in Lynch et al. (1997) with a time span of 3.5 h and a pass-band edge of 5 h: the associated transfer function is shown in Fig. 1. Moreover, the surface analysis is performed based on the final trajectory valid at T/2 (Giard and Bazile 2000). The background field for the next assimilation is obtained by integrating this analysis up to the beginning of the next assimilation interval, that is, $t = T$.

The assimilation uses all observations currently assimilated operationally at Météo-France. These include conventional observations like radiosondes (TEMP and PILOT), aircraft reports (AIREPs), and a variety of surface observations over land and sea. The total amount of data ingested by the system is of the order of 10^4 including cloud-cleared (Television Infrared Observation Satellite) TIROS Operational Vertical Sounder (TOVS) radiances. Observations have been collected in 1-h time slots except for a few surface observations and buoys. As discussed in Järvinen et al. (1999), these require the introduction of time correlations in the observational errors that were not considered in our treatment of the observations. In the terminology of Rabier et al. (2000), this is the distinction between the so-called 3D and 4D screening.

Here, the focus will be on the impact of introducing the digital filter as a weak constraint in the manner explained in the previous section. The incremental model is Eulerian and uses a time step of 900 s. The weights used in the J_c-DFI were those associated with a Dolph filter with a 6-h time span and a 3-h pass-band edge. Referring to Fig. 1, the transfer function is seen to be less dissipative than that of the operational external DFI. It is not as efficient to filter out oscillations with periods between 4 and 6 h. On the other hand, it does not damp the waves as much in the pass band.

5. Comparative experiments between the digital filter and normal-mode formulations

Imposing a constraint will degrade the fit of the analysis to the observations compared to a minimization without any constraint. To illustrate this, three experiments were carried out with the incremental 4DVAR as described above. These experiments used, respectively, no penalty term (No-J_c), a penalty term based on the NNMI (J_c-NMI), and one based on the DFI (J_c-DFI). In the case of the J_c-NMI, it is important to stress once more that, at the final outer iteration, an external DFI was performed on the high-resolution analysis increments to yield the final high-resolution trajectory. Figure 3 shows the reduction in the J_o cost function as a function of iteration: the solid and long-dashed lines correspond, respectively, to the J_c-NMI and J_c-DFI experiments while the short-dashed one is for the No-J_c experiment. The triangles and squares indicate the value of the cost function for an outer iteration when the observations are compared against the high-resolution trajectory. What this figure shows is that even though the inner iterations improve the fit to the observations, this improvement may not be representative of the actual fit of the high-resolution trajectory resulting from adding the low-resolution increment to the high-resolution reference initial conditions. This is clearly seen at iteration 50 when an outer iteration is performed.

In the J_c-NMI experiment, the application of the external DFI results in a final fit to the observations that is worse than that obtained at the previous outer itera-

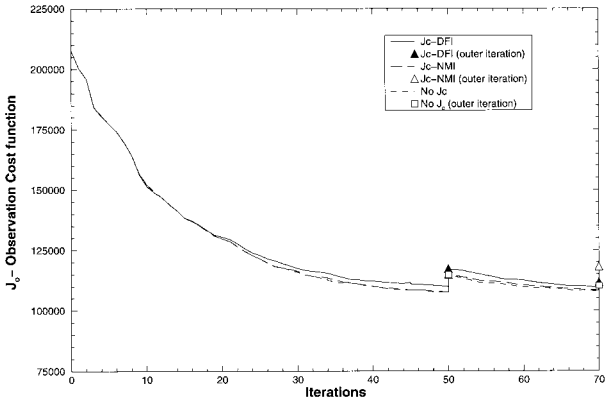

FIG. 3. Impact of the imposition of a weak constraint on the observation cost function during the miminization. Solid (J_c-DFI) and dashed (J_c-NMI) lines are associated with inner iterations while the black (J_c-DFI) and white (J_c-NMI) triangles indicate the value of the cost function obtained at an outer iteration. Both analyses were initiated from the same background field that was used to initiate the assimilation cycle on 8 Jan 1999 at 0000 UTC.

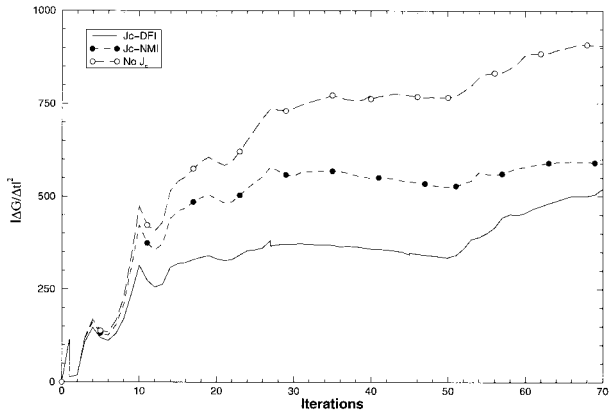

FIG. 4. Norm of gravity wave tendency when no weak constraint is applied (No J_c), when J_c-NMI and J_c-DFI are used.

tion. It is also noticeable that during the first inner loop, the J_c-NMI allows a closer fit to the observations than the J_c-DFI does. In fact, the results with the J_c-NMI are very close to what is obtained with no constraint at all, which may be indicative that it is not very successful at constraining the emergence of fast oscillations. Finally, at the final iteration, it is quite clear that the application of the external DFI pushes the solution further away from the observations while, with the J_c-DFI, the final fit of the high-resolution trajectory compares well with that of the case with no constraint.

To show if the resulting analysis is devoid of fast oscillations, the norm of the tendency of gravity waves $|\partial \mathbf{G}/\partial t|$ can be used as a measure of gravity wave activity that corresponds to the very formulation of the J_c-NMI (Courtier and Talagrand 1990). Figure 4 represents J_c-NMI as a function of iteration for the three experiments described above. It shows that the J_c-DFI manages to constrain more of the emergence of gravity waves than the direct use of the J_c-NMI. During the first 20 iterations, the tendency of the gravity waves increases until saturation, the penalty term preventing any further increase. However, even when no J_c is introduced, a similar behavior occurs except that the saturation occurs at a higher level. Finally, after an outer iteration (at iteration 50), the balance is upset and the level of gravity wave activity starts increasing again.

By varying the penalty constant λ, it is possible to control the degree to which the constraint is imposed. Several experiments were carried out to find out what would be an appropriate choice for λ. For those experiments, we used a lower horizontal resolution so that the high-resolution model was at T95L31C3.5 and the incremental model at T63L31C1.0. Time series of surface pressure over a 6-h interval are presented in Fig. 5. The reference experiment is one in which no constraint was imposed and no DFI was done on the final high-resolution analysis increments (thin solid line marked by circles). The J_c-NMI without the DFI at the end does not constrain the minimization very much and its solution follows very closely that of the reference. Applying the DFI on the final analysis increment (thick solid line marked with asterisks) reduces the amplitude of fast oscillations but the solution differs significantly from the unconstrained experiment, which fits better the observations. It is interesting to note that the J_c-DFI with $\lambda = 100$ yields a solution that agrees relatively well with that obtained by performing the external DFI. However, this increases unduly the relative importance of the J_c with respect to that of J_b. With a value of $\lambda = 10$, the relative importance of J_c compared to J_b was 20% and this was considered reasonable. Consequently, the fast oscillations are not completely filtered (see Fig. 5) but their amplitudes are reduced to a level that lies in between the DFI solution and the unconstrained case.

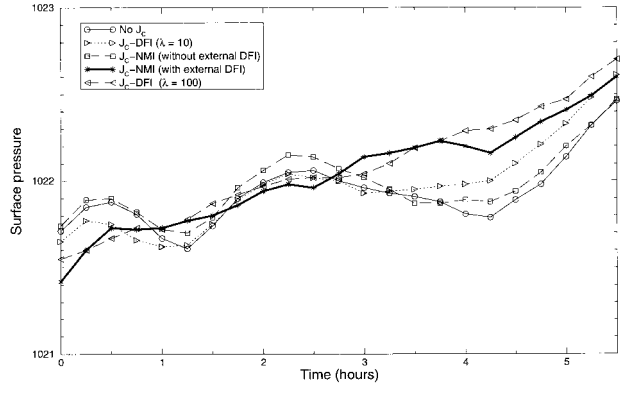

FIG. 5. Time series of surface pressure (at 47°N, 14°W) over a period of 6 h for a preliminary experiment setup at a lower resolution of T95L31C3.5 and T63L31C1.0. The heavy solid line represents the reference time series (J_c-NMI with DFI) for which a digital filter initialization was applied on the high-resolution increment. Two experiments used the J_c-DFI with the penalty constant set to $\lambda = 10$ and $\lambda = 100$. Also shown: an experiment without any J_c (No J_c) and the J_c-NMI without applying the DFI on the final high-resolution analysis increments.

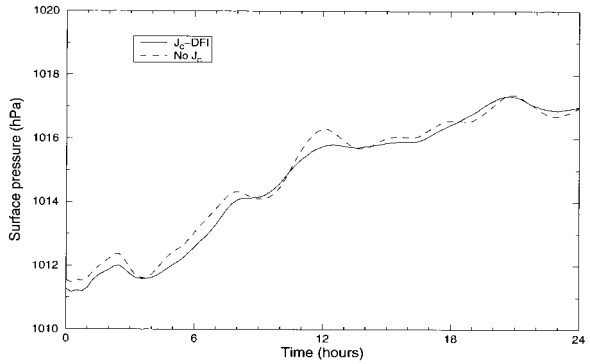

FIG. 6. Time series of surface pressure (at 49°N, 4°W) over a 24-h period. Solid (dashed) line represents the integration from the J_c-DFI (No J_c) experiment. These results are based on the preoperational configuration described in section 3.

This conclusion holds for the preoperational configuration as shown in Fig. 6: only the cases without constraint (No J_c) and the J_c-DFI with $\lambda = 10$ are presented.

The spectra of the divergence analysis increments are shown in Fig. 7 at levels corresponding approximately to 233 and 869 hPa: these correspond to the increments of the incremental model at a T95L31C1.0 uniform resolution. This confirms our earlier findings that the J_c-NMI experiment differs very little from the experiment without any constraint. The high-resolution increments are defined over the transformed sphere and their spectra are representative of what is going on over the high-resolution region of ARPEGE. Moreover, the J_c-NMI experiment shows the impact of the external DFI on the analysis increments. These spectra are represented in Figs. 8 and 9 at $t = -3$ and 0 h, respectively; the latter time corresponding to the analysis time from which the ARPEGE forecasts are made. At the initial time, the analysis increments should not contribute significantly to the small scales since the increments are defined at a much lower resolution. Figure 8 shows that the external DFI does have an impact on the small-scale components, damping them at 233 hPa but increasing them at 869 hPa. This may be explained by the fact that the DFI as described in Lynch et al. (1997) involves a backward integration of an adiabatic version of the model followed by a forward integration of the complete model from $t = -3$. So even though only the large scales are changed by the analysis, this can have an influence on the small scales. What is noticeable is that 3 h seem to suffice to damp these initial differences between the J_c-NMI and J_c-DFI, the spectra being very similar at the analysis time (Fig. 9). At that time, one observes that compared to the case without any constraint and DFI, the differences subsist mostly in the large scales.

Finally, the divergence increments at 850 hPa are shown over western Europe in Figs. 10 (No J_c), 11 (J_c-DFI), and 12 (J_c-NMI with external DFI) at $t = -3$ and 0 h. Comparing Figs. 10 and 11 shows that J_c-DFI reduces very slightly the amplitude of the divergence

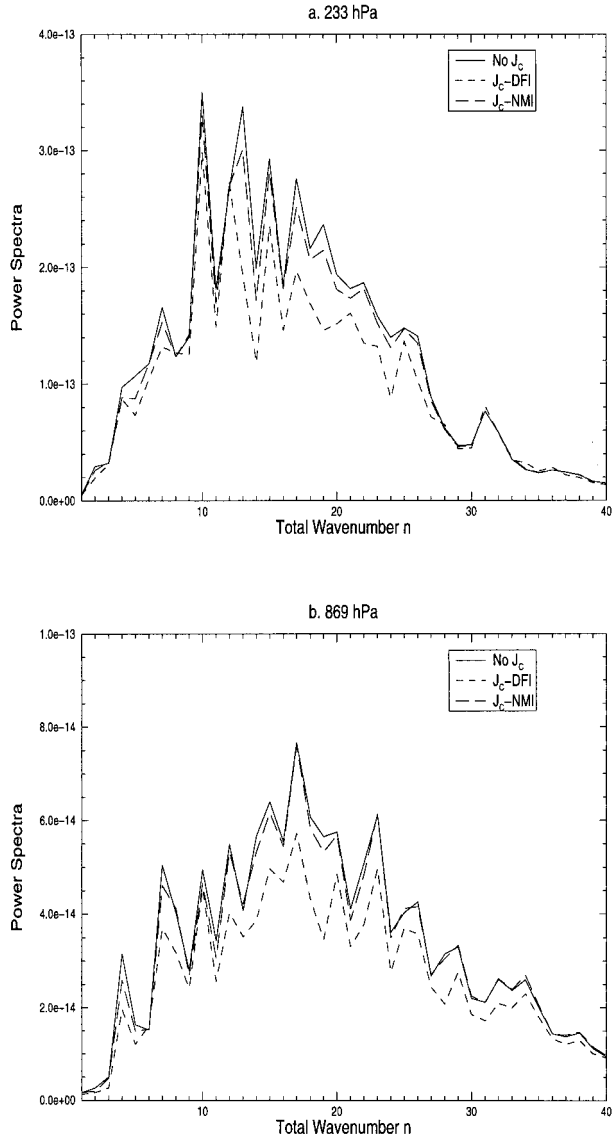

FIG. 7. Spectra of divergence of the low-resolution analysis increments at (a) 233 and (b) 869 hPa. The cases of no constraint (No J_c), J_c-DFI, and J_c-NMI are shown.

while Fig. 12 indicates that the external DFI alters significantly the shape of the analysis increments. For instance, this is particularly apparent west of the Alps both at $t = -3$ and 0 h.

The results presented in this section assess the impact of different formulations on a static analysis in which the background field used as the initial point of the minimization is identical in all cases. In the next section, a comparison will be made of the results obtained in the context of a 2-week assimilation cycle.

6. Impact on the forecasts

To assess the impact on the forecasts, assimilation cycles were carried out from 9 to 25 January 1999, a

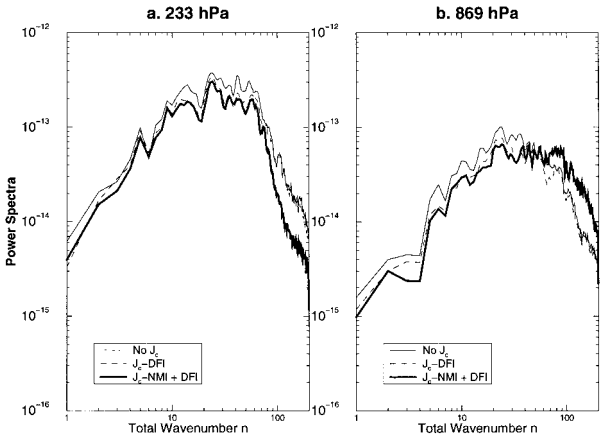

FIG. 8. Divergence power spectra at (a) 233 and (b) 869 hPa. The spectra have been computed over the transformed sphere (T199L31C3.5) at the beginning of the assimilation interval and are therefore representative of the divergence field over the high-resolution portion of the ARPEGE domain.

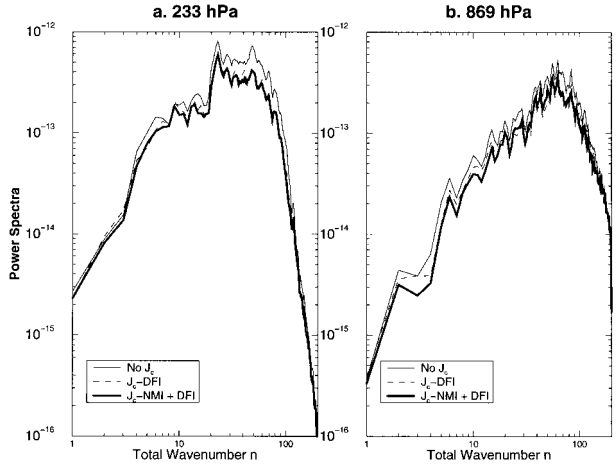

FIG. 9. As in Fig. 8 but 3 h later, which corresponds to the middle of the assimilation interval.

period used to test the preoperational 4DVAR. Four experiments have been compared: the three previously described (No J_c, J_c-DFI, and J_c-NMI) and a control corresponding to a similar cycle based on the operational 3DVAR, which included an external DFI on the analysis increments. These three 4DVAR experiments were first compared to assess the necessity of filtering fast oscillations. Figure 13 shows the verification of the 6-h forecasts with radiosonde data over the Northern Hemisphere for the whole period. In this comparison, J_c-DFI and J_c-NMI behave very similarly but removing any type of constraint (No J_c) introduces a significant error particularly evident for the zonal wind component. This negative impact observed for all quantities convinced us of the necessity of constraining the emergence of fast oscillations even in the context of 4DVAR.

Preliminary experiments were carried out to assess the impact of 4DVAR on the forecasts based on these analyses. The baseline being the operational 3DVAR system (Thépaut et al. 1998), a control experiment was also performed using 3DVAR for the analysis: a digital filter initialization is applied to the analysis increments. This system slightly differs from the operational system at that time in that TOVS radiances were also included. The ''control'' experiment was chosen to be close to what is expected to be the reference when 4DVAR will be tested against the operational suite. Since then, this particular version of 3DVAR was implemented operationally at Météo-France in March 1999. In 3DVAR, all the observations within the -3 to $+3$ h assimilation window are grouped in the single slot centered at 0 h, while in 4DVAR, they are collected in 1-h time slots so that the forecast is compared with observations closer to the exact observation time.

Forecasts were made every day at 0000 UTC and 17 cases were obtained and verified against the operational analyses every 24 h. The overall conclusion is that there is a clear positive impact of 4DVAR. Figure 14 shows the rms error of the vector wind at 250 hPa over Europe. The verification being made with respect to the operational 3DVAR analysis, the control experiment has a

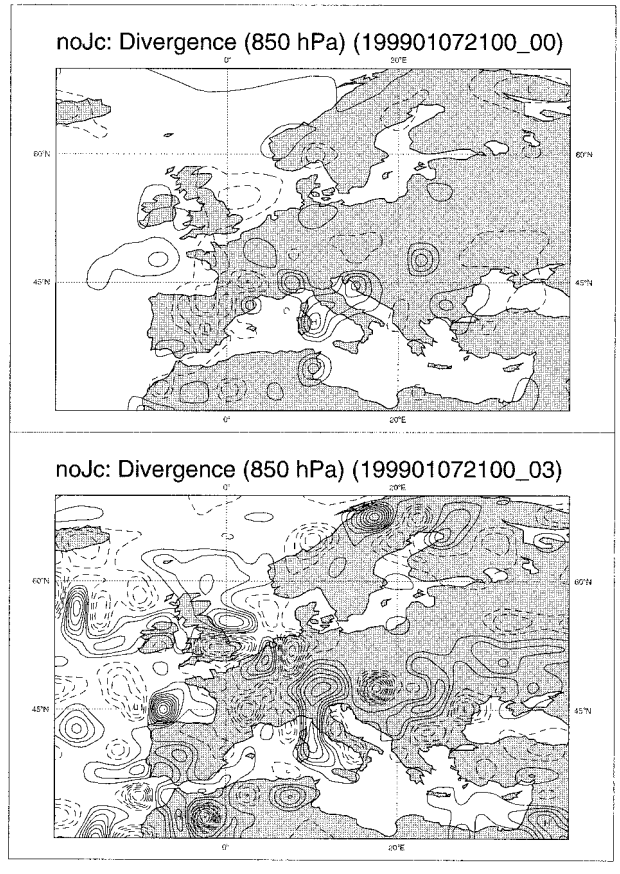

FIG. 10. Analysis increments on divergence at 850 hPa when no constraint is applied on the fast oscillations. Results are shown at the (top) beginning and (bottom) middle of the assimilation interval, which starts on 21 Jan 2000 at 0000 UTC.

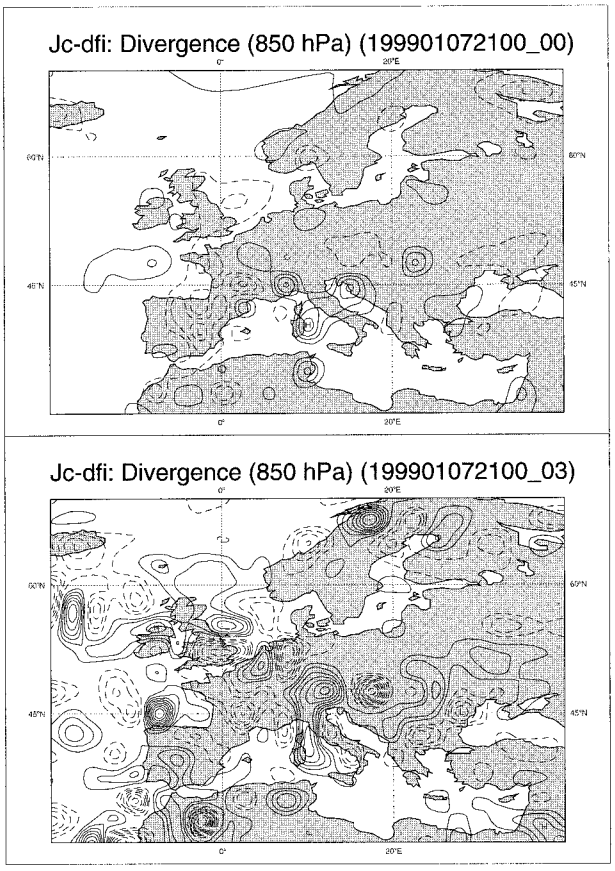

FIG. 11. As in Fig. 10 but when a J_c-DFI constraint is imposed.

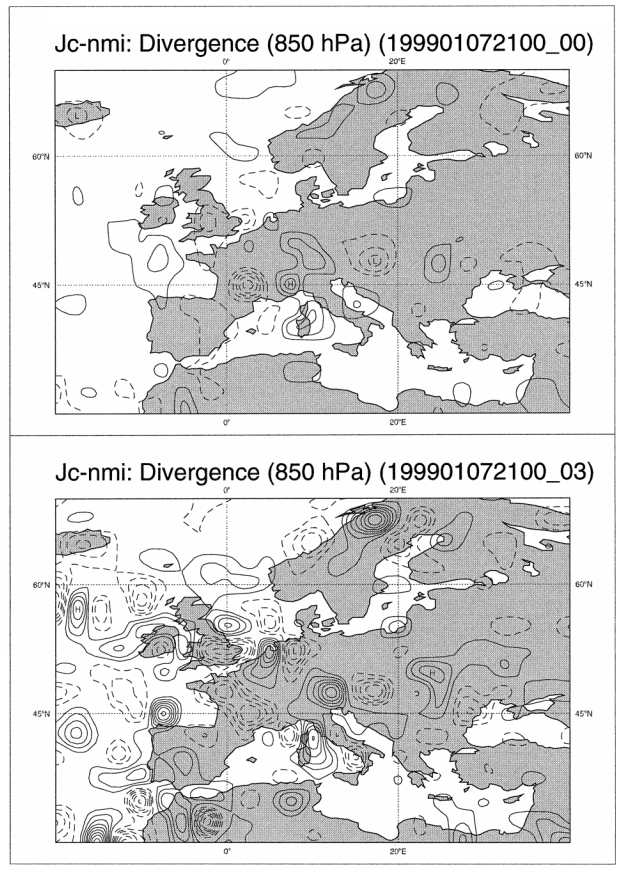

FIG. 12. As in Fig. 10 but when a J_c-NMI constraint is imposed and an external digital filter initialization is applied at the initial time of the final trajectory.

significantly smaller error that does not persist after 24 h. The three 4DVAR experiments show equivalent results, the differences not being statistically significant.

Fast oscillations are filtered primarily because of their impact on the vertical motion that in turn affects precipitation. This leads to the so-called spinup period at the beginning of the forecast during which the model relaxes toward its internal dynamical balance. This manifests itself in the precipitation patterns and in differences between the initial tendencies and those obtained in the midst of the integration. Precipitation rates have been computed and averaged over the 17 forecasts of each experiment. Figure 15 shows that the three 4DVAR experiments retained do not exhibit imbalances comparable to those observed in the analyses obtained with the 3DVAR system. The results also show that the J_c-DFI constraint seems as able to remove the spinup as is the application of an external DFI, while fitting more closely the observations as shown earlier.

To measure the degree of imbalance at the initial time, the time and space averages of the physical tendencies have been computed as

$$x(T) = \frac{1}{T}\int_0^T \left\langle \frac{\partial \mathbf{X}}{\partial t} \right\rangle dt,$$

which is the time average of the physical tendencies of the model. Here, x stands for either kinetic energy, geopotential, temperature, or specific humidity. The notation $\langle\cdot\rangle$ represents the spatial average over a given area. Figure 16 compares the difference between $x(T)$ at 6 h and that at 72 h $[x(72) - x(6)]$ for kinetic energy, temperature, geopotential, and specific humidity averaged over the Northern Hemisphere. Again the three 4DVAR experiments come out as being more in balance when compared to the 3D-Var experiment. There is no convincing evidence that either the J_c-NMI or J_c-DFI constraint improves significantly the degree of balance in 4DVAR, which naturally imposes the dynamical constraint since the fit to the observations is made by adjusting a model trajectory. Without any constraint (No J_c), the innovation statistics at 6 h show however a significant degradation (see Fig. 13).

In summary, these experiments have shown that the J_c-DFI is able to control sufficiently the emergence of fast oscillations and the spinup, while keeping the analysis closer to the observations than is possible when applying an external DFI. From a practical point of view, the application of the external DFI requires supplementary integrations of the high-resolution model

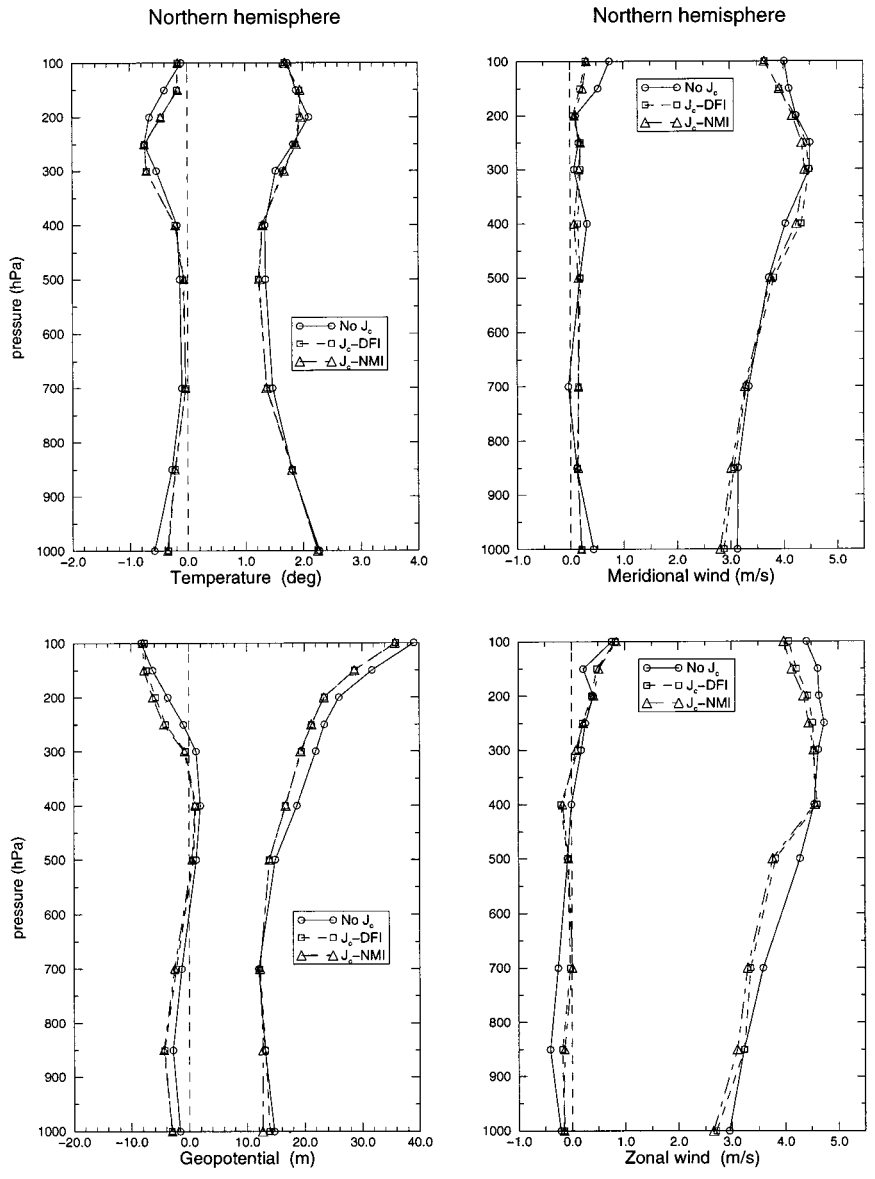

FIG. 13. Verification of the 6-h forecasts against radiosonde data over the Northern Hemisphere: (upper left) rms error and biases are shown for temperature, (upper right) meridional wind, (lower left) geopotential, and (lower right) zonal wind component. These have been computed for the same period and for three 4DVAR experiments: No J_c, J_c-NMI, and J_c-DFI.

and moreover, the computation of the J_c-NMI itself is adding an extra cost. This combines to 12%–15% of the total cost of one 4DVAR analysis while, as shown here, the cost of the J_c-DFI is virtually null. Moreover, it must be pointed out that the normal mode initialization cannot be applied in the context of the stretched geometry of the ARPEGE model without introducing costly computations.

7. Discussion and conclusions

The digital filter initialization is a simple method to filter out spurious fast oscillations in a forecast due to imbalances introduced by the analysis. In the context of a 3D data assimilation scheme, it has the disadvantage of adding the computing cost associated with a supplementary model integration of approximately 4.5 h. Applying the DFI over a limited time span also damps waves with periods longer than those that need to be filtered and the filter can only be sharpened by increasing the time span, which would add to its cost. Another problem with the DFI is that it is difficult to obtain a filtered analysis at the exact analysis time without resorting to some approximations. Finally, applying a DFI on the final analysis increments deteriorates the fit to the observations. In this paper, it has been shown that

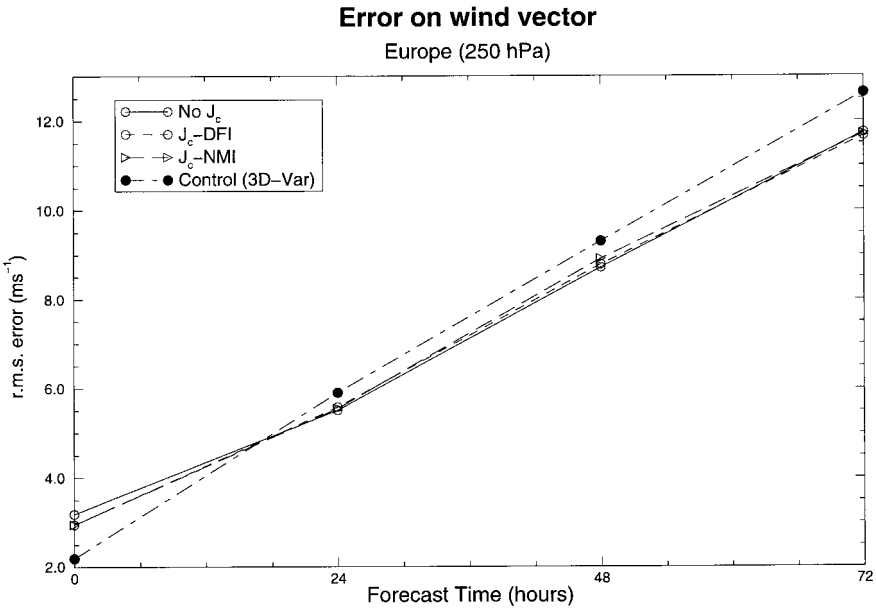

FIG. 14. Verification of forecasts every 24 h against the operational analyses. Rms error on wind vector has been averaged over the period 9–22 Jan 1999.

in the context of 4DVAR, many of these difficulties disappear by using a weak constraint formulation. Since the time span of the DFI now corresponds to the assimilation window of 4DVAR, the application of the DFI through the J_c-DFI will become naturally more selective when 4DVAR is performed over a 12- or even 24-h period. In that case, as shown in Fig. 2, a Dolph window formulation is significantly less dissipative in the pass band and is more appropriate than the Dolph filter used in our experiments. The weak constraint formulation of the DFI proposed here presents other advantages. It easily allows control of the degree to which the constraint is imposed in the course of the 4DVAR minimization. This significantly improves the fit to the observations in the final analysis while obtaining an analysis that reduces the level of spurious fast oscillations comparable to what is obtained by imposing the DFI after the fact. Another benefit is that the J_c-DFI adds only a negligible cost to the 4DVAR assimilation process. Removing the external DFI has reduced the cost of the

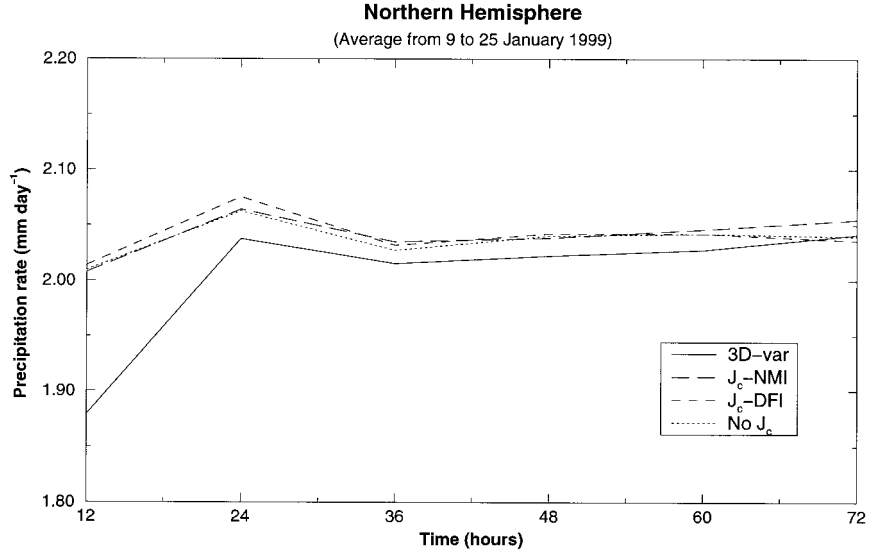

FIG. 15. Average precipitation rates (in mm day^{-1}) as a function of forecast time, which have been averaged over the Northern Hemisphere for the 2 week period extending from 9 to 25 Jan 1999.

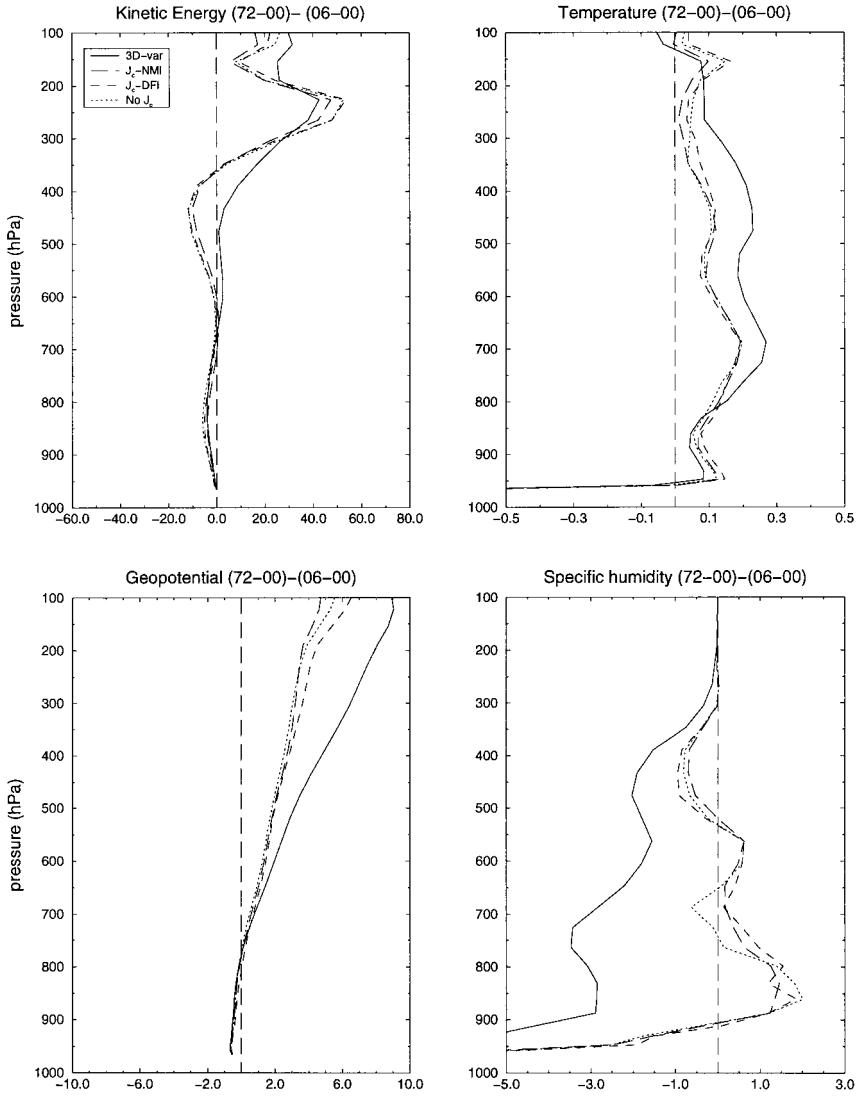

FIG. 16. Differences in tendencies averaged over the Northern Hemisphere midlatitudes for (a) kinetic energy, (b) temperature, (c) geopotential, and (d) specific humidity ($\times 10^5$). The solid line corresponds to the 3DVAR experiment, the long- and short-dashed lines to the J_c-NMI and J_c-DFI experiments, respectively.

preoperational[1] 4DVAR assimilation by 12%–15%. Finally, it is encouraging to note that as the assimilation window is increased, the DFI tends toward the ''idealized'' filter (see Fig. 2) that does not damp slower oscillations. It has also been shown that the use of a Dolph window instead of a Dolph filter is preferable.

The impact of the J_c-DFI has been assessed in the context of assimilation cycles of 2 weeks and these experiments have shown that it is just as capable as the external DFI of maintaining the internal balance within the model while improving the fit to the observations. The degree of imbalance has been measured by the spinup in the precipitation rate in the first 24 h of integration and by the differences in tendencies at 6 and 72 h averaged in space and time. The results show, on average, a neutral impact on the forecasts at a range of 24–72 h. It is also important to stress that without any type of constraint, the 4DVAR analyses still exhibit a significantly reduced degree of initial imbalance compared to what is currently present in 3DVAR analyses.

In the absence of any external constraint on the analysis increments, the current background error covariances impose an approximate form of balance on the increments that is close to a linear balance relationship. With new forms of flow-dependent covariances such as those proposed in Fisher (1998) based on a reduced-

[1] The 4DVAR assimilation system became operational at Météo-France on 20 June 2000 in a form that is very close to that used in the J_c-DFI experiment.

rank Kalman filter, constraining the analysis may become more of a necessity. It may also be the case when more sophisticated physical parameterization schemes are introduced in the inner iterations (Janisková et al. 1999).

Acknowledgments. The authors would like to acknowledge the help of François Bouyssel who performed the diagnostics presented in section 6. We particularly thank Dominique Giard for her careful and detailed review of our manuscript. Thanks also to Jean-François Geleyn for several discussions who helped us to better understand the impact of digital filtering. Comments by Stéphane Laroche, Saroja Polavarapu, Florence Rabier, Monique Tanguay, and two anonymous reviewers helped to improve the final version of the manuscript.

The first author would also like to express his appreciation to the staff of the Groupe de Modélisation pour l'Assimilation et la Prévision (GMAP) for their help in making his stay at Météo-France a fruitful one.

REFERENCES

Ballish, B., X. Cao, E. Kalnay, and M. Kanamitsu, 1992: Incremental nonlinear normal-mode initialization. *Mon. Wea. Rev.,* **120,** 1723–1734.

Courtier, P., and J.-F. Geleyn, 1988: A global numerical weather prediction model with variable resolution: Application to the shallow-water equations. *Quart. Meteor. Soc.,* **114,** 1321–1346.

——, and O. Talagrand, 1990: Variational assimilation of meteorological observations with the direct and adjoint shallow-water equations. *Tellus,* **42A,** 531–549.

——, C. Freydier, J. F. Geleyn, F. Rabier, and M. Rochas, 1991: The ARPEGE project at Météo-France. *Proc. ECMWF Seminar on Numerical Methods in Atmospheric Models,* Reading, United Kingdom, ECMWF.

——, J. N. Thépaut, and A. Hollingsworth, 1994: A strategy for operational implementation of 4D-Var, using an incremental approach. *Quart. J. Roy. Meteor. Soc.,* **120,** 1367–1387.

——, and Coauthors,1998: The ECMWF implementation of three dimensional variational assimilation (3D-Var). Part I: Formulation. *Quart. J. Roy. Meteor. Soc.,* **124,** 1783–1808.

Derber, J., and F. Bouttier, 1999: A reformulation of the background error covariance in the ECMWF global data assimilation system. *Tellus,* **51A,** 195–221.

Ehrendorfer, M., R. M. Errico, and K. D. Raeder, 1999: Singular-vector perturbation growth in a primitive equation model with moist physics. *J. Atmos. Sci.,* **56,** 1627–1648.

Fillion, L., H. L. Mitchell, H. R. Ritchie, and A. N. Staniforth, 1995: The impact of a digital filter finalization technique in a global data assimilation system. *Tellus,* **47A,** 304–323.

Fisher, M., 1998: Development of a simplified Kalman filter. ECMWF Tech. Memo. 260, 16 pp.

Gauthier, P., C. Charette, L. Fillion, P. Koclas, and S. Laroche, 1999: Implementation of a 3D variational data assimilation system at the Canadian Meteorological Centre. Part I: The global analysis. *Atmos.–Ocean,* **37,** 103–156.

Geleyn, J. F., and Coauthors,1994: Atmospheric parameterization schemes in Météo-France's ARPEGE numerical weather prediction model. *Proc. ECMWF Seminar on Parameterization of Sub-gridscale Physical Processes,* Reading, United Kingdom, ECMWF, 385–402.

Giard, D., and E. Bazile, 2000: Implementation of a new assimilation scheme for soil and surface variables in a global NWP model. *Mon. Wea. Rev.,* **128,** 997–1015.

Gustafsson, N., 1992: Use of a digital filter as weak constraint in variational data assimilation. *Proc. ECMWF Workshop on Variational Assimilation with Special Emphasis on Three-dimensional Aspects,* Reading, United Kingdom, ECMWF, 327–338.

Hamming, R. W., 1989: *Digital Filters.* Prentice-Hall, 284 pp.

Janisková, M., J.-N. Thépaut, and J.-F. Geleyn, 1999: Simplified and regular physical parameterizations for incremental four-dimensional variational assimilation. *Mon. Wea. Rev.,* **127,** 26–45.

Järvinen, H., E. Andersson, and F. Bouttier, 1999: Variational assimilation of time sequences of surface observations with serially correlated errors. *Tellus,* **51A,** 468–487.

Laroche, S., and P. Gauthier, 1998: A validation of the incremental formulation of 4D variational data assimilation in a nonlinear barotropic flow. *Tellus,* **50A,** 557–572.

Lynch, P., 1997: The Dolph–Chebyshev window: A simple optimal filter. *Mon. Wea. Rev.,* **125,** 655–660.

——, and X. Y. Huang, 1992: Initialization of the HIRLAM model using a digital filter. *Mon. Wea. Rev.,* **120,** 1019–1034.

——, D. Giard, and V. Ivanovici, 1997: Improving the efficiency of a digital filtering scheme for diabatic initialization. *Mon. Wea. Rev.,* **125,** 1976–1982.

Polavarapu, S., M. Tanguay, and L. Fillion, 2000: Four dimensional variational data assimilation with digital filter initialization. *Mon. Wea. Rev.,* **128,** 2491–2510.

Puri, K., W. Bourke, and R. Seaman, 1982: Incremental linear normal mode initialization in four-dimensional data assimilation. *Mon. Wea. Rev.,* **110,** 1773–1785.

Rabier, F., H. Järvinen, E. Klinker, J.-F. Mahfouf, and A. Simmons, 2000: The ECMWF operational implementation of four dimensional variational assimilation. Part I: Experimental results with simplified physics. *Quart. J. Roy. Meteor. Soc.,* **126,** 1143–1170.

Thépaut, J.-N., and Coauthors,1998: The operational global data assimilation system at Météo-France. *Proc. HIRLAM4 Workshop on Variational Analysis in Limited Area Models,* Toulouse, France, 25–31 pp.

Veersé, F., and J.-N. Thépaut, 1998: Multiple truncation incremental approach for four-dimensional variational data assimilation. *Quart. J. Roy. Meteor. Soc.,* **124,** 1889–1908.